Contents

As a special case we consider stirrups as ties with $\alpha = \pi/2$ and a strut inclination $\theta = \pi/4$. This leads to a shear stiffness

$$\frac{\partial V}{\partial \gamma} = \frac{1}{4}\, zb\, E_c = \frac{1}{2}\, zb\, G_c \tag{3.165}$$

with the shear modulus G_c according to Eq. (3.8). We compare this with the linear elastic case, Eq. $(3.13)_3$, with a geometry coefficient α. Here a relation $zb = \alpha_c\, A$, $\alpha_c = z/h$ is used with a similar geometry coefficient α_c. Thus, relations $(3.13)_3$ and (3.165) differ by a factor of 2. In the current argument, concrete tensile struts are disregarded due to the limited tensile strength of concrete and shear reinforcement was assumed as vertical stirrups, which do not directly contribute to V. Thus, the current setup and the linear elastic case coincide for $\theta = \pi/4$.

There is some margin to choose the concrete shear strut angle, see [26, 6.2.3], [18, 7.3.3.3]. The limits are roughly by a range $20° \leq \theta \leq 45°$. As a first estimation, the same strut angle should be used as for the design of the stirrups.

3.6 Prestressing

Prestressing applies lateral redirection forces and normal forces on a beam, see Fig. 3.14. While the redirection forces act against dead and variable loads a moderate normal force may increase the bearing capacity for moments, see Example 3.1. But these positive effects involve demands for prestressing tendons. A concrete beam and its untensionend reinforcement on one hand and the tendons with high strength steel on the other hand are regarded as separated structural elements in the following.

Originally, the generalized stress $\boldsymbol{\sigma}$ is formulated as a function of the generalized deformations $\boldsymbol{\epsilon}$, e.g.,

$$\boldsymbol{\sigma} = \mathbf{C} \cdot \boldsymbol{\epsilon} \tag{3.166}$$

For $\mathbf{C}$ see, e.g., Eq. (3.140). The linearity of $\mathbf{C}$ is not necessarily required. This concept is extended with respect to prestressing, i.e., an additional part is assigned to the generalized stresses resulting from *prestressing tendons*

$$\boldsymbol{\sigma} = \mathbf{C} \cdot \boldsymbol{\epsilon} + \boldsymbol{\sigma}^p \tag{3.167}$$

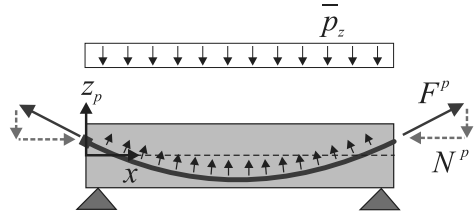

Figure 3.14: Redirection forces from prestressing.

This additional part depends on the tendon profile. In the case of the Bernoulli beam

$$\boldsymbol{\sigma}^p = \begin{pmatrix} N^p \\ M^p \end{pmatrix} = -F^p \begin{pmatrix} \cos\alpha_p \\ -z_p\,\cos\alpha_p \end{pmatrix} \tag{3.168}$$

compare Eq. (3.68), with the prestressing force F^p, the height coordinate or lever arm z_p of the tendon, and the inclination $\alpha_p = \mathrm{d}z_p/\mathrm{d}x$ of the tendon against the beam reference axis. This may be extended with respect to shear forces in combination with the Timoshenko beam. Using the extended generalized stresses (Eq. (3.167)) for the internal nodal forces (Eq. (3.101)) leads to a split

$$\mathbf{f}_e = \int_{L_e} \mathbf{B}^T \cdot \boldsymbol{\sigma}\,\mathrm{d}x = \int_{L_e} \mathbf{B}^T \cdot \mathbf{C} \cdot \boldsymbol{\epsilon}\,\mathrm{d}x + \int_{L_e} \mathbf{B}^T \cdot \boldsymbol{\sigma}^p\,\mathrm{d}x = \mathbf{f}_e^\epsilon + \mathbf{f}_e^p \tag{3.169}$$

The part $-\mathbf{f}_e^p$ may be regarded as a further contribution to the load vector, see Eq. (1.69). This approach integrates prestressing in the given framework whereby all procedures but for a part of load evaluation remain unchanged.

An alternative and conventional view of prestressing of beams is based on Eq. (3.58). We consider the quasistatic case, split internal forces into a part $\bullet^\epsilon$ from beam deformation, a part $\bullet^p$ from prestressing and eliminate shear forces

$$\begin{aligned} -N^{\epsilon\prime} - N^{p\prime} &= \bar{p}_x \\ -M^{\epsilon\prime\prime} - M^{p\prime\prime} &= \bar{p}_z \end{aligned} \tag{3.170}$$

Furthermore, Eq. (3.168) is used leading to

$$\begin{aligned} -N^{\epsilon\prime} &= \bar{p}_x - (F^p \cos\alpha_p)' \\ -M^{\epsilon\prime\prime} &= \bar{p}_z + (z_p F^p \cos\alpha_p)'' \end{aligned} \tag{3.171}$$

The weak form of these differential equations, see Section 3.2, conforms to Eqs. (3.167, 3.168).

A common approximation is $F^p \approx const.$, $\cos\alpha_p \approx 1$ resulting in

$$-M^{\epsilon\prime\prime} = \bar{p}_z + z_p'' F^p \tag{3.172}$$

wherein $z_p'' F^p$ is a lateral redirection force in the z-direction from the curvature z_p'' of the tendon geometry. This term may be seen as an additional lateral loading counteracting the other loadings, see Fig. 3.14 with negative $\bar{p}_z$.

Some characteristic properties of prestressing have to be regarded for the evaluation of $\boldsymbol{\sigma}_p$ or $\mathbf{f}^p$, respectively:

- Tendon profile parameters z_p, α_p may vary with the beam coordinate x according to prestressing design.

- The prestressing force may vary due to the loss of prestress from friction of the tendon in a conduit.

– Furthermore, a beam deformation may lead to a change in the tendon profile after application and fixing of prestressing. Two cases have to be considered:

1. *Prestressing without bond*: total length of the tendon changes. This leads to a global change of the prestressing force.
2. *Prestressing with bond*: length of the tendon changes locally to keep the geometric compatibility with the concrete. This leads to locally varying changes in the prestressing force.

Two subsequent stages have to be considered for prestressing:

– Application stage of prestressing with the prescribed prestressing force F_0^p

  Prestressing is gradually applied at a beam's ends through anchors. The value of F_0^p may vary along the longitudinal beam coordinate x due to friction losses. Such losses have to determined from prescribed friction coefficients and the curvature of the tendon geometry. Tendons are grouted at the end of this stage in the case of prestressing with bond.

– Fixed stage of prestressing with locked anchors

  The prestressing force F_0^p changes into F_p according to the enumeration above concerning with/without bond. Different approaches are necessary to describe the global or local change of the tendon geometry for the both cases in this stage.

The tendon geometry plays a key role within this context. It may be described for each finite beam element in analogy to the Bernoulli beam shape function (Eq. (3.76)) with

$$z_p = \left[\frac{r^3}{4} - \frac{3r}{4} + \frac{1}{2} \quad \frac{L_e r^3}{8} - \frac{L_e r^2}{8} - \frac{L_e r}{8} + \frac{L_e}{8} \quad -\frac{r^3}{4} + \frac{3r}{4} + \frac{1}{2} \quad \frac{L_e r^3}{8} + \frac{L_e r^2}{8} - \frac{L_e r}{8} - \frac{L_e}{8}\right] \cdot \begin{pmatrix} cz_{pI} \\ \alpha_{pI} \\ z_{pJ} \\ \alpha_{pJ} \end{pmatrix} \tag{3.173}$$

with the element length L_e and the tendon inclination

$$\alpha_P = \frac{\partial z_p}{\partial x} = \frac{\partial z_p}{\partial r}\frac{\partial r}{\partial x} = z_p' \tag{3.174}$$

Lateral tendon position and inclination on the left- and right-element end are given by z_{pI}, α_{pI} and z_{pJ}, α_{pJ}. The local element coordinate is in the range $-1 \leq r \leq 1$. This approach reproduces $z_p(-1) = z_{pI}$, $z_p'(-1) = \alpha_{pI}$ and $z_p(1) = z_{pJ}$, $z_p'(1) = \alpha_{pJ}$. The geometric length of tendon in an element e is given by

$$L_e^P = \frac{L_e}{2}\int_{-1}^{1} \sqrt{(x_p')^2 + (z_p')^2}\ \mathrm{d}r \tag{3.175}$$

whereby the derivative of the tendon position x_p in the longitudinal direction has also to be regarded. Equation (3.175) has to be integrated numerically for each element, e.g., with a Gauss integration, see Section 1.6.

Equation (3.173) for tendon geometry is on one hand applied to the nominal undeformed tendon geometry according to design with

$$\begin{pmatrix} x'_p \\ z_{pI} \\ \alpha_{pI} \\ z_{pJ} \\ \alpha_{pJ} \end{pmatrix} = \begin{matrix} 1 \\ \begin{pmatrix} z_{p0I} \\ \alpha_{p0I} \\ z_{p0J} \\ \alpha_{p0J} \end{pmatrix} \end{matrix} \tag{3.176}$$

with the prescribed values $z_{p0I}, \alpha_{p0I}, z_{p0J}, \alpha_{p0J}$. On the other hand, Eq. (3.173) gives the tendon geometry considering beam deformation with

$$\begin{pmatrix} x'_p \\ z_{pI} \\ \alpha_{pI} \\ z_{pJ} \\ \alpha_{pJ} \end{pmatrix} = \begin{matrix} 1+\epsilon \\ \begin{pmatrix} z_{p0I} + w_I \\ \alpha_{p0I} + \phi_I \\ z_{p0J} + w_J \\ \alpha_{p0J} + \phi_J \end{pmatrix} \end{matrix} \tag{3.177}$$

with the longitudinal strain ϵ of the beam's reference axis and the beams nodal displacements w_I, ϕ_I, w_J, ϕ_J. The total length L^P of a tendon is computed by adding all element contributions.

Regarding prestressing *without bond*, the tendon length can be determined separately for application stage, with a value L_0^P, and for the fixed stage with a value L^P. Equations (3.175, 3.177) can be used with the appropriate deformations or displacements, respectively. Regarding Eq. (3.168), this leads to a prestressing force

$$F^p = \frac{L^P}{L_0^P} F_0^p \tag{3.178}$$

in the fixed stage of prestressing.

Regarding prestressing *with bond* a tendon gets a local elongation after fixing of prestressing due to bond. This local elongation is ruled by the beam's deformation kinematics equation (3.5), i.e., the additional strain of the tendon is given by

$$\Delta\epsilon_p(x) = \Delta\epsilon(x) - z_p \, \Delta\kappa(x) \tag{3.179}$$

with the variable values $\Delta\epsilon$, $\Delta\kappa$ of the beam deformations during the fixed stage of prestressing. This leads to to a prestressing force

$$F^p(x) = F_0^p + E_p A_p \, \Delta\epsilon_p(x) \tag{3.180}$$

with Young's modulus E_p of the prestressing steel, the cross section area A_p of prestressing tendons and $F^p(x)$ used in Eq. (3.168).

The particular procedures concerning prestressing can be summarized as follows:

- Define the tendon geometry and prestressing force
- Compute internal forces from prestressing

- Compute nodal loads from prestressing
- Compute system reaction
- Iterate if neccessary to capture changing in prestressing force

The application is demonstrated with the following example.

Example 3.6 Prestressed RC beam
We refer to Example 3.2 with basically the same system, but the span is doubled to $L = 10$ m. Thus, the structure's load bearing capacity is strongly reduced. Prestressing is used to increase the bearing capacity. The relevant system parameters are as follows:

- A concrete cross section $b = 0.2, h = 0.4$, a compressive strength $f_{cd} = 38\,\mathrm{MN/m^2}$ and a lower and upper reinforcement $A_{s1} = A_{s2} = 12.57\,\mathrm{cm^2}$, $d_1 = d_2 = 5\,\mathrm{cm}$ yield an ultimate bending moment $M_u \approx 0.20\,\mathrm{MNm}$ with $N = 0$, see Example 3.1. This corresponds to a uniform loading $q_u = 8M_u/L^2 = 15.2\,\mathrm{kN/m}$ which should be increased by prestressing.
- A nominal uniform concrete prestressing stress of $\sigma_{c0} = -10\,\mathrm{MN/m^2}$ is chosen in a first approach leading to $F_0^p = 0.8\,\mathrm{MN}$. The nominal tendon geometry of the whole beam is given by a parabola starting and ending in the center line with a downward camber h_p. This is described by
$$z_p = 4h_p \left(\frac{x^2}{L^2} - \frac{x}{L} \right) \tag{3.181}$$
A value $h_p = 0.15\,\mathrm{m}$ is chosen in this example.
- Prestressing tendon and steel properties are chosen with a cross section area $A_p = 6\,\mathrm{cm^2}$, elastic limit $f_{p0,1} = 1600\,\mathrm{MN/m^2}$, strength $f_p = 1800\,\mathrm{MN/m^2}$, and Young's modulus $E_p = 200\,000\,\mathrm{MN/m^2}$. Nominal initial steel stress is $\sigma_0^p = 1\,333\,\mathrm{MN/m^2}$ with a strain $\epsilon_0^p = 6.67$ ‰.
- A dead load is assumed with $q = 5\,\mathrm{kN/m}$.

Loading is applied in two stages: (1) Application of prestressing and dead load, (2) fixing of prestressing and additional application of a service load $q_p = 25\,\mathrm{kN/m}$. Frictional losses are neglected to simplify this example. Both cases – prestressing with and without bond – are alternatively regarded for the fixed stage of prestressing. The solution method is incrementally iterative with Newton–Raphson iteration within increments.

This leads to the following results for prestressing *without* bond:

- The computed increase in prestressing force after load step 2 according to Eq. (3.178) is minimal with $F^p/F_0^p = 1.002$. This results from the low ratio $h_p/L = 1/67$.
- For the computed mid-span displacements, see Fig. 3.15a. The deflection starts with an uplift during application of prestressing. The final mid-span deflection is quite large with 0.113 m ($\approx 1/90$ of the span), but the load-carrying capacity is not yet exhausted with an upper mid-span concrete compressive strain of -2.2 ‰(limit strain is -3.5 ‰). Serviceability is presumably not given without further provisions due to high slenderness (1/25).

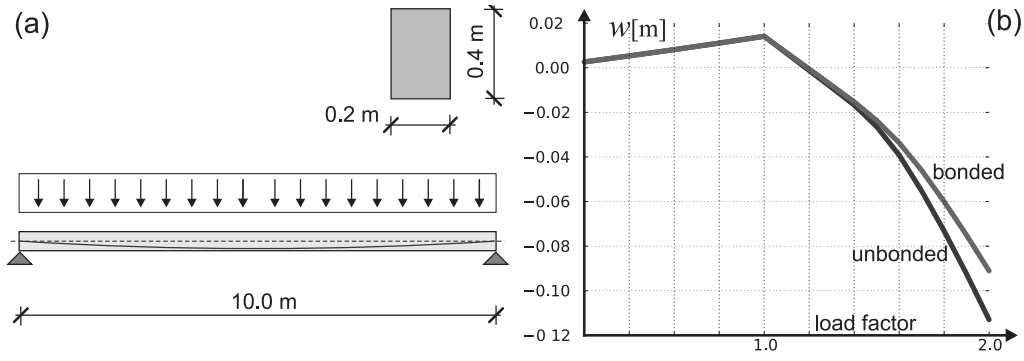

Figure 3.15: Example 3.6 (a) System (b) Mid-span load–deflection curve.

– For the bending moment and normal force in the RC cross section, see Fig. 3.16a. Total moment from the dead load weight and the service load is $M_q = 0.03 \times 10^2/8 = 0.375\,\text{MNm}$. The computed RC mid-span contribution is $M_c = 0.255$ and the contribution from prestressing $M_p = 0.120$. The increased RC moment compared to the initial estimation results from the compressive normal force.

Furthermore, the results for prestressing *with* bond:

– In the case of bond, the tendon gets a local additional strain due to the locally varying deformation of the beam, see Eq. (3.179). This leads to an additional prestressing force, see Eq. (3.180) and Fig. 3.16b, and in the end to higher contribution of prestressing to load bearing capacity and a higher total load bearing capacity.

– Detail results are given by final mid-span deflection 0.12 m, see Fig. 3.15b, RC moment contribution $M_c = 0.220$, see Fig. 3.16a, contribution from prestressing $M_p = 0.155$.

Prestressing roughly leads to a doubling of ultimate limit loads in this example. Aspects of serviceability have to be treated separately.

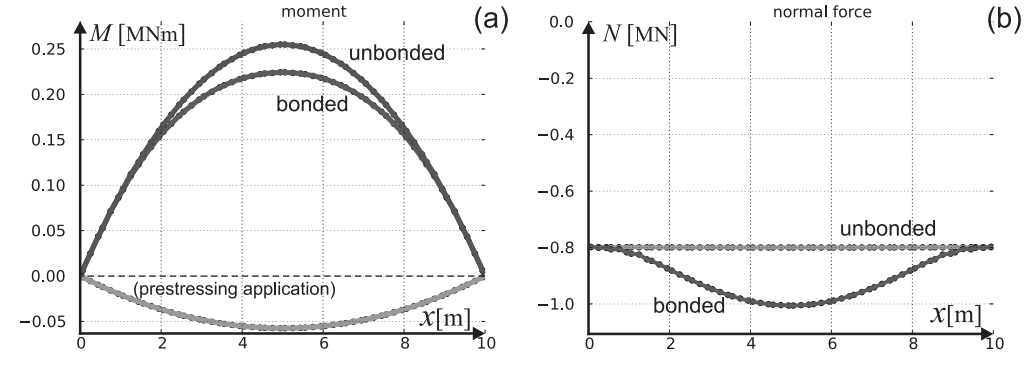

Figure 3.16: Final stage Example 3.6 (a) RC bending moment. (b) RC normal force.

The comparison between prestressing with and without bond in this example is somehow academic, as in practice prestressing with bond is exposed to more nonmechanical effects, which might lead to some restrictions to fully utilize the load carrying capacities of the prestressing steel. Details are ruled in codes.

End Example 3.6

Some remarks concerning prestressing remain to be added. All methods and procedures may be also applied to material laws of a rate type, see Eq. (1.50), instead of Eq. (3.166) within an incrementally iterative scheme, see Section 1.6.

Prestressing may be superposed with creep of concrete (Section 3.5.1), temperature and shrinkage (Section 3.5.2), and tension stiffening (Section 3.5.3). All described approaches are compatible and may be used in any combination. The application has been demonstrated in Example 3.6 for a single-span beam which is statically determinate.

- Methods and procedures in same way may be applied to statically indeterminate systems as solution procedures always simultaneously regard equilibrium, material behavior, and kinematic compatibility.

High strength steel is used for prestressing with roughly three times the strength of ordinary rebar steel. Relaxation, see Section 2.2, occurs for such types of steel. The approach of, e.g., Eq. (2.27) can basically be used for the phenomena of creep and relaxation and in a first approach for steel as well as for concrete. It can be also applied to the prestressing force F^p, see Eq. (3.168), leading to a transient analysis as in a similar way has already been discussed in Section 3.5.1.

3.7 Large Deformations and Second-Order Analysis

Up to now, we considered the equilibrium of structures in their undeformed configuration. The displacements of a structure were neglected in the balance of external actions and internal forces and a *geometrically linear analysis* was performed. This is justified for RC beams which are exposed to predominant bending or tension. Structural deformations generally will not have an appreciable influence on internal forces in such cases. This might change for structural members exposed to compression. Depending on their slenderness internal forces may considerably increase due to structural deformations and deformations have to be considered regarding equilibrium. This leads to *geometrical nonlinearities*.

We consider a section of a plane beam in some deformed configuration, see Fig. 3.17. A quasistatic analysis shall be performed whereby equilibrium should be given in the deformed configuration. Thus, the integration of the equilibrium condition (Eq. (3.65)) of a section of length L

$$\int_0^L \delta\boldsymbol{\epsilon}^T \cdot \boldsymbol{\sigma}\, \mathrm{d}s = \int_0^L \delta\mathbf{u}^T \cdot \bar{\mathbf{p}}\, \mathrm{d}s + \delta\mathbf{U}^T \cdot \bar{\mathbf{t}} \tag{3.182}$$

has to be performed in the deformed configuration with the coordinate s along the beam axis. It is appropriate to relate the generalized stresses $\boldsymbol{\sigma}$ and the generalized strains $\boldsymbol{\epsilon}$, see Eqs. (3.66, 3.68), to a local *corotational coordinate system*. A single element is considered in the following which is straight in the undeformed configuration.

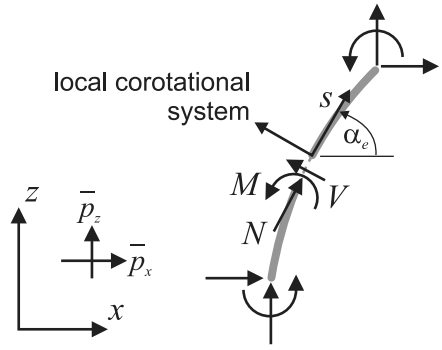

Figure 3.17: Equilibrium of beam section in the deformed configuration.

- It is assumed that the curvature of a single element is still small in the deformed configuration and that its deformed geometry can be approximated with a straight line connecting its end nodes.

This assumption is appropriate for RC structures failing with relatively small strains. Furthermore, the deformed geometry may be approximated with any desired accuracy by refining the discretization.

The corresponding element orientation is given by the angle α_e. Global nodal degrees of freedom $\boldsymbol{v}_e$ are transformed to the local system with Eq. (3.109)

$$\tilde{\boldsymbol{v}}_e = \mathbf{T}(\alpha_e) \cdot \boldsymbol{v}_e \tag{3.183}$$

Local displacements and strains are given according to Eqs. (3.78, 3.81)

$$\tilde{\mathbf{u}}(r) = \mathbf{N}(r) \cdot \tilde{\boldsymbol{v}}_e, \quad \boldsymbol{\epsilon}(r) = \mathbf{B}(r) \cdot \tilde{\boldsymbol{v}}_e \tag{3.184}$$

leading to virtual strains

$$\delta\boldsymbol{\epsilon}^T = \delta\boldsymbol{v}_e^T \cdot \mathbf{T}^T(\alpha_e) \cdot \mathbf{B}^T(r) \tag{3.185}$$

Internal nodal forces of a beam element are given by Eqs. (3.101, 3.110)

$$\mathbf{f}_e = \mathbf{T}^T(\alpha_e) \cdot \frac{L_e}{2} \int_{-1}^{1} \mathbf{B}^T(r) \cdot \boldsymbol{\sigma}(r)\, \mathrm{d}r \tag{3.186}$$

with the actual element length L_e whereby the orientation α_e depends – beneath the initial coordinates of the element's nodes – on the values of the nodal degrees of freedom or displacements, respectively.

- With the internal nodal forces depending on the deformation the problem becomes geometrically nonlinear. This is combined with physical nonlinearity in the case of RC beams due to the nonlinear behavior between the generalized strains and stresses.

The evaluation of the tangential stiffness is mandatory for such problems. The tangential element stiffness matrix is determined by

$$\mathbf{K}_{Te} = \frac{\partial \mathbf{f}_e}{\partial \boldsymbol{v}_e} \tag{3.187}$$

see Eq. (1.64). Regarding Eq. (3.186) this leads to

$$\mathbf{K}_{Te} = \mathbf{K}_{TMe} + \mathbf{K}_{TGe} \tag{3.188}$$

with the tangential stiffness contribution from material behavior

$$\begin{aligned} \mathbf{K}_{TMe} &= \mathbf{T}^T \cdot \frac{L_e}{2} \int_{-1}^{1} \mathbf{B}^T \cdot \frac{\partial \boldsymbol{\sigma}}{\partial \boldsymbol{\epsilon}} \cdot \frac{\partial \boldsymbol{\epsilon}}{\partial \tilde{\boldsymbol{v}}_e} \cdot \frac{\partial \tilde{\boldsymbol{v}}_e}{\partial \boldsymbol{v}_e} \, \mathrm{d}r \\ &= \mathbf{T}^T \cdot \frac{L_e}{2} \int_{-1}^{1} \mathbf{B}^T \cdot \mathbf{C}_T \cdot \mathbf{B} \, \mathrm{d}r \cdot \mathbf{T} \\ &= \mathbf{T}^T \cdot \widetilde{\mathbf{K}}_{Te} \cdot \mathbf{T} \end{aligned} \tag{3.189}$$

according to Eqs. (1.65, 3.114) and furthermore with the tangential stiffness contribution from geometry

$$\mathbf{K}_{TGe} = \frac{\partial \mathbf{T}^T}{\partial \alpha_e} \cdot \tilde{\mathbf{f}}_e \cdot \frac{\partial \alpha_e}{\partial \boldsymbol{v}_e}^T \tag{3.190}$$

with the local internal nodal forces

$$\tilde{\mathbf{f}}_e = \frac{L_e}{2} \int_{-1}^{1} \mathbf{B}^T \cdot \boldsymbol{\sigma} \, \mathrm{d}r \tag{3.191}$$

Regarding the Bernoulli beam element, see Section 3.3.2 and Eq. (3.111), the factors of Eq. (3.190) are given by

$$\frac{\partial \mathbf{T}^T}{\partial \alpha_e} = \begin{bmatrix} -\sin\alpha_e & -\cos\alpha_e & 0 & 0 & 0 & 0 \\ \cos\alpha_e & -\sin\alpha_e & 0 & 0 & 0 & 0 \\ 0 & 0 & 0 & 0 & 0 & 0 \\ 0 & 0 & 0 & -\sin\alpha_e & -\cos\alpha_e & 0 \\ 0 & 0 & 0 & \cos\alpha_e & -\sin\alpha_e & 0 \\ 0 & 0 & 0 & 0 & 0 & 0 \end{bmatrix} \tag{3.192}$$

and

$$\tilde{\mathbf{f}}_e = \begin{pmatrix} N_I \\ V_I \\ M_I \\ N_J \\ V_J \\ M_J \end{pmatrix}, \qquad \frac{\partial \alpha_e}{\partial \boldsymbol{v}_e} = \frac{1}{L_e} \begin{pmatrix} \sin\alpha_e \\ -\cos\alpha_e \\ 0 \\ -\sin\alpha_e \\ \cos\alpha_e \\ 0 \end{pmatrix} \tag{3.193}$$

This leads to a geometric tangential element stiffness

$$\mathbf{K}_{TGe} = \begin{bmatrix} -A_I \sin\alpha_e & A_I \cos\alpha_e & 0 & A_I \sin\alpha_e & -A_I \cos\alpha_e & 0 \\ B_I \sin\alpha_e & -B_I \cos\alpha_e & 0 & -B_I \sin\alpha_e & B_I \cos\alpha_e & 0 \\ 0 & 0 & 0 & 0 & 0 & 0 \\ -A_J \sin\alpha_e & A_J \cos\alpha_e & 0 & A_J \sin\alpha_e & -A_J \cos\alpha_e & 0 \\ B_J \sin\alpha_e & -B_J \cos\alpha_e & 0 & -B_J \sin\alpha_e & B_J \cos\alpha_e & 0 \\ 0 & 0 & 0 & 0 & 0 & 0 \end{bmatrix} \tag{3.194}$$

for the two-node Bernoulli beam element with

$$A_i = \sin\alpha_e N_i + \cos\alpha_e V_i, \quad B_i = \cos\alpha_e N_i - \sin\alpha_e V_i, \quad i = I, J \tag{3.195}$$

Internal nodal forces from Eq. (3.186) have to be in equilibrium with the external nodal forces. External nodal forces for distributed loading are determined in analogy to Eq. (3.105) leading to

$$\bar{\mathbf{p}}_e = \frac{L_e}{2} \int_{-1}^{1} \mathbf{T}^T(\alpha_e) \cdot \mathbf{N}^T(r) \cdot \mathbf{Q}(\alpha_e) \cdot \bar{\mathbf{p}}(r)\, \mathrm{d}r \tag{3.196}$$

with the vector rotation matrix $\mathbf{Q}$, see Eq. (C.6), and for the boundary terms with Eq. (3.106)

$$\bar{\mathbf{t}}_e = \begin{pmatrix} \bar{N}_I & \bar{V}_I & \bar{M}_I & \bar{N}_J & \bar{V}_J & \bar{M}_J \end{pmatrix}^T \tag{3.197}$$

for the two-node Bernoulli beam element. The components of $\bar{\mathbf{t}}_e$ and $\bar{\mathbf{p}}$, see Eq. (3.66), are related to the global coordinate system. The extended Bernoulli beam element, see Section 3.3.2, and the Timoshenko beam elements, see Section 3.3.3, can be treated in the same way with the adaption of $\boldsymbol{\upsilon}_e$, $\boldsymbol{\epsilon}$, $\boldsymbol{\sigma}$ and $\mathbf{T}$.

The system equations are assembled from the element contributions, as is described in Section 1.5, leading to a condition for quasistatic equilibrium

$$\mathbf{f}(\boldsymbol{\upsilon}) = \mathbf{p} \tag{3.198}$$

with $\mathbf{p} = \bar{\mathbf{p}} + \bar{\mathbf{t}}$, compare Eq. (1.60). The solution is determined with an incrementally iterative scheme, see Section 1.6, whereby the tangential stiffness should include material stiffness and geometric stiffness as are given for single elements with Eqs. (3.189, 3.190).

The described approach corresponds to a *corotational updated Lagrangian* discretization [9, 4.4, 4.6]. It may be applied to cases with large deformations and small strains. *Second-order analysis* is included as a special case whereby displacements are linearized with respect to an initially undeformed configuration. A first validation is given by the following example.

Example 3.7 Stability limit of cantilever column

We consider a simple cantilever column with linear elastic behavior and a discretization with one two-node Bernoulli beam element, see Fig. 3.18. It has a vertical concentrated load at its top acting along the axis of gravity. A buckling from the initial configuration or instability will occur within a theory regarding equilibrium in deformed configurations. The buckling load shall be determined for this simple model.

The model has three degrees of freedom with u, w, ϕ at the top node. The initial configuration is given by $\alpha_e = \pi/2$. The material stiffness is determined by Eq. (3.189) with $\mathbf{B}$ from Eq. (3.82), $\mathbf{C}_T = \mathbf{C}$ from Eq. (3.16) and $\mathbf{T}$ from Eq. (3.111) with α_e replacing α. This yields

$$\mathbf{K}_{TM} = \begin{bmatrix} \frac{12EJ}{L^3} & 0 & \frac{6EJ}{L^2} \\ 0 & \frac{EA}{L} & 0 \\ \frac{6EJ}{L^2} & 0 & \frac{4EJ}{L} \end{bmatrix} \tag{3.199}$$

for the actual degrees of freedom. The geometric stiffness according to Eq. (3.194) is determined by

$$\mathbf{K}_{TG} = \bar{N}_J\, \mathbf{K}^0_{TG}, \qquad \mathbf{K}^0_{TG} = \begin{bmatrix} \frac{1}{L} & 0 & 0 \\ 0 & 0 & 0 \\ 0 & 0 & 0 \end{bmatrix} \tag{3.200}$$

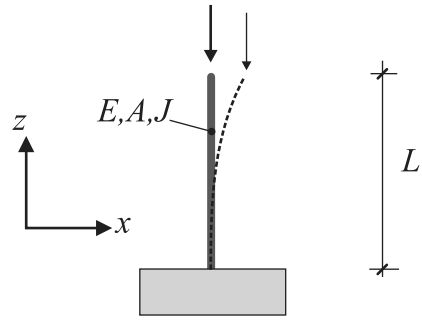

Figure 3.18: Cantilever column.

The matrix $\mathbf{K}_{TG}^{0}$ is independent from loading and covers the geometry of the initial undeformed configuration.

The incremental system behavior is described by Eq. (1.66)

$$(\mathbf{K}_{TM} + \mathbf{K}_{TG}) \cdot \mathrm{d}\boldsymbol{v} = \mathrm{d}\mathbf{f} \tag{3.201}$$

- An instability is given by *nonzero* increments of displacements $\mathrm{d}\boldsymbol{v}$ in connection with *zero* increments of nodal forces $\mathrm{d}\mathbf{f}$.

This leads to the generalized eigenvalue problem

$$\mathbf{K}_{TM} \cdot \mathrm{d}\boldsymbol{v} = -N_{Jb}\ \mathbf{K}_{TG}^{0} \cdot \mathrm{d}\boldsymbol{v} \tag{3.202}$$

with the buckling load N_{Jb}. The solution for this model is

$$N_{Jb} = \frac{3\,EJ}{L^2} \tag{3.203}$$

whereby the relation between lateral displacement and rotation is determined with $9\tilde{w}_J + 6L\,\phi = 0$. The exact solution is given by $\pi^2\,EJ/4L^2 \approx 2.47\,EJ/L^2$ according to the well-known Euler cases for buckling. The error in N_{Jb} results from the discretization with one element which is a rough approximation of the exact cosine solution. A refinement of the discretization should improve the solution for N_{Jb}.

End Example 3.7

The method described for the stability analysis of a cantilever column is based on the generalized eigenvalue problem (3.202). It may be applied to all types of columns and frames with compressive members in the undeformed configuration. Furthermore, the approach may be generalized for the stability analysis of all types of structures [9, 6.5].

Up to now, we regarded linear elastic material behavior. The nonlinear behavior of cracked RC cross sections, see Section 3.1.3, has to be considered in the next step. This will be described for Bernoulli beams in the following.

A deformed configuration is given within an incremental iterative scheme, see Section 1.6, with an orientation angle α_e and an actual length L_e for each element. Generalized strains

$\boldsymbol{\epsilon}$ and generalized stresses $\boldsymbol{\sigma}$ or internal forces, see Eq. (3.68), are determined in the local corotational system. With the generalized strains given the internal forces are determined from Eqs. (3.22, 3.23) and the tangential stiffness $\mathbf{C}_T$ from Eq. (3.55). This yields the basic quantities required for the internal nodal forces in the global system (Eq. (3.186)), the tangential material stiffness (Eq. (3.189)) and the tangential geometric stiffness (Eq. (3.194)). The external nodal forces in the global system are finally determined from Eqs. (3.196, 3.197) for a new loading target. Prescribed displacements are treated as described in Section 3.4.3. The nonlinear problem – including the continuing updating of α_e, L_e – is solved by, e.g., the Newton–Raphson method, see Eqs. (1.71, 1.72).

The application is demonstrated with the following example.

Example 3.8 Ultimate limit for RC cantilever column

The stability of the cantilever column has already been treated in Example 3.7 as a buckling or the generalized eigenvalue problem whereby resembling the classical Euler case. This assumes a centered load without eccentricity and a linear elastic material behavior and leads to an upper bound for the load carrying capacity. A load eccentricity and the nonlinear behavior of a cracked RC sections are considered while regarding large displacements or second order effects, respectively. Geometry, discretization, and boundary conditions are as follows:

- Cantilever column with a height $L = 5.0\,\mathrm{m}$, square cross section with width $h = 0.4\,\mathrm{m}$ and a depth $b = 0.2\,\mathrm{m}$, see Fig. 3.6a.
- Discretization with $n_E = 10$ extended two-node Bernoulli beam elements, see Section 3.3.2.
- The bottom node is clamped with zero displacements and zero rotations.

The column is assumed to be stabilized in the out-of-plane direction. The material properties and the reinforcement are chosen as with Example 3.1:

- Concrete grade C30/37 according to [26, Table 3.1] with an initial Young's modulus $E_c = 33\,000\,\mathrm{MN/m^2}$. Concrete compressive strength is assumed with $f_c = 38\,\mathrm{MN/m^2}$ with $\epsilon_{c1} = -0.0023$, $\epsilon_{cu1} = -0.0035$, see Fig. 2.1. A tensile strength is disregarded. The uniaxial stress–strain relation is chosen according to [26, 3.1.5].
- Reinforcement behavior is assumed according to Section 2.3 and [26, 3.2.7] with $f_{yk} = 500\,\mathrm{MN/m^2}$, $f_t = 525\,\mathrm{MN/m^2}$, $\epsilon_{y0} = 2.5‰$ and $\epsilon_u = 25‰$, see Fig. 2.10a.
- Left and right reinforcement each with a geometry $4 \oslash 20$, $A_{s2} = A_{s1} = 12.57\,\mathrm{cm^2}$, $d_2 = d_1 = 5\,\mathrm{cm}$.

The elastic in-plane stability limit or buckling load is determined as

$$P_b = \frac{\pi^2}{4}\,\frac{EJ}{L^2} = \frac{\pi^2}{4}\,\frac{33\,000 \cdot 0.001067}{5.0^2} = 3.47\,\mathrm{MN} \tag{3.204}$$

The vertical downward load target is chosen with $P = 2\,\mathrm{MN}$ with an eccentricity of $e = 0.032\,\mathrm{m}$, see Fig. 3.19a. The moment–curvature for this compressive force has been determined in Example 3.1 and is shown in Fig. 3.3.

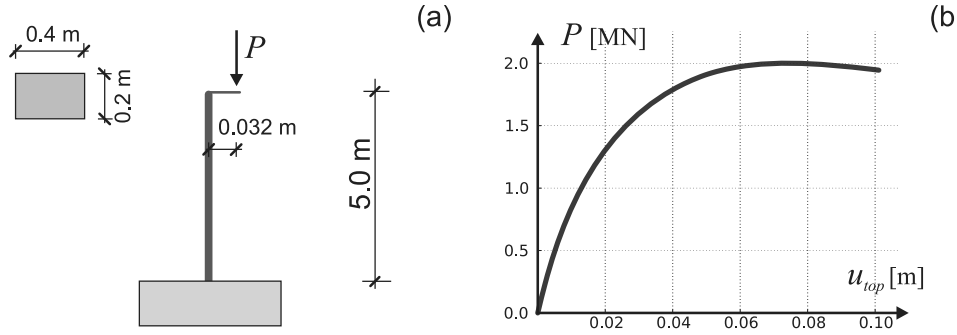

Figure 3.19: Example 3.8 (a) System (b) Vertical load–horizontal displacement relation.

An incrementally iterative scheme with arc length control to determine load increments, see Appendix A, and Newton–Raphson iteration within each loading increment, see Section 1.6, is used as the solution method. The computation leads to the following results:

– The computed relation between horizontal top displacement and vertical load is shown in Fig. 3.19b. It is nonlinear due to both geometrical and physical nonlinearities. The prescribed maximum is reached with a horizontal displacement of $u_u = 0.071\,\text{m}$. The vertical load has to be reduced for larger horizontal displacements to maintain equilibrium in the deformed configuration. The arc length method is mandatory to model this structural softening behavior effect.

  A load value of $P = 2\,\text{MN}$ cannot be reached with initial eccentricities $e > 0.032\,\text{m}$ as the structural softening behavior will start with lower loads.

– The computed moments along the column are shown in Fig. 3.20a for different loading factors. The computed top moment $M_{z=4.94} = 0.067\,\text{MNm}$ corresponds to the prescribed eccentricity moment of $e\,P \rightarrow 0.064\,\text{MNm}$. In the same way the computed bottom moment $M_{z=0.06} = 0.206\,\text{MNm}$ corresponds to the prescribed plus

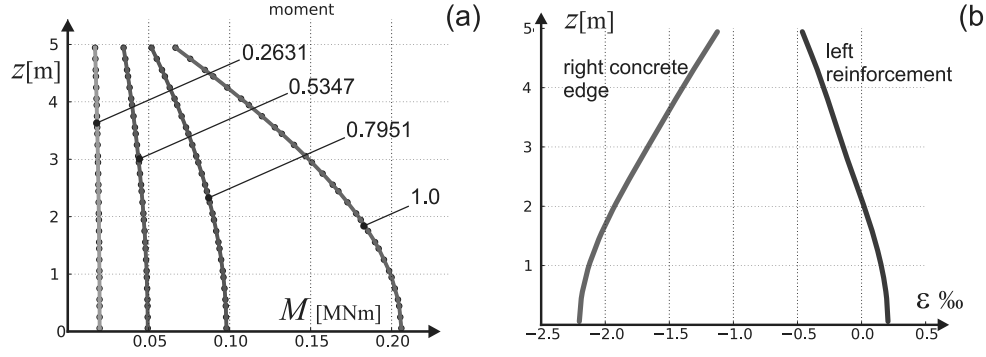

Figure 3.20: Example 3.8 (a) Moments along column. (b) Strains along column.

deformation eccentricity moment $(e + u_u)\, P \rightarrow 0.206\,\text{MNm}$. This exceeds the moment from first-order theory by the factor of 3.2. Using a linear elastic material behavior with $E = 33\,000\,\text{MN/m}^2$ would lead to a stiffer behavior with a moment $M_{x=0.06} = 0.172\,\text{MNm}$.

The maximum bottom bending moment connected to the ultimate structural load is considerably lower compared to the ultimate cross-sectional moment of $M_u = 0.261\,\text{MNm}$, see Example 3.1 with Fig. 3.3, indicating a structural instability.

– Strain distributions along the column for the left-reinforcement and the right-concrete edge are shown in Fig. 3.20b for the final loading state. The materials limit strains – e.g., $\epsilon_{cu1} = -0.0035$ for concrete – are not reached although the system has reached its limit load.

The cantilever column is the most important case for second order computations for RC structures. But the described approach may also be directly applied to other types of columns and to all kinds of plane multistory frames.

End Example 3.8

Considering certain effects like some amount of tensile strength or tension stiffening will increase the stiffness of the model. Tension stiffening may be regarded with a modification of the stress–strain relation for the reinforcement, see Section 3.5.3. A value for the tensile strength is considered with the lower and upper compression zone coordinates z_{c1}, z_{c2}, see Section 3.1.3.1, with an extended definition of the zero line z_0, see Eqs. (3.19, 3.20).

On the other hand, an effect like creep will increase the deformations and also the internal forces in the deformed configuration. But the load level should be lower as only a permanent or quasi-permanent loading will lead to creep. The approach for creep as is described in Section 3.5.1 can be combined with the method for large displacements to investigate creep effects.

3.8 Dynamics of Beams

Dynamic actions on structures may arise from walking pedestrians, vehicular traffic, rotating machines, wind, seismicity, impact, and explosions. Decisive is a structure's largest *natural period* compared to a characteristic time of an action. Such characteristic times may come from the step frequency of pedestrians, velocity of vehicles, rotational frequency of machines, frequency of gusts or ground motions, duration of impact and explosions. If the largest natural period of a structure is not considerably smaller than the characteristic action time a structure's inertia comes into play. The manifold aspects of dynamics of civil engineering structures are treated by, e.g., [10], [37], [53].

Basics of inertia for beams are given in Eqs. (3.58, 3.65), which introduce the inertial mass m per unit length of a beam and the inertial mass moment Θ. In the case the center line of area coincides with the beam's reference axis, see Section 3.1.1, they are given by

$$m = \varrho\, A, \quad \Theta = \varrho\, J \tag{3.205}$$

with the material's specific mass ϱ, the cross-sectional area A and the second moment of area J. If the center line of area does not coincide with the reference axis the definition of Θ has

to be modified. On the other hand, contributions connected with the inertial mass moment Θ are often neglected, as they are relatively small. Some care should be given to the units.

- Specific mass ϱ has to be distinguished from specific weight, i.e., a given specific weight has to be divided by earth acceleration.

Appropriate methods to solve dynamic problems have already been laid down. The basic approach for a discretized system is given by Eq. (1.90)

$$\mathbf{M} \cdot \ddot{\boldsymbol{v}}(t) + \mathbf{f}(t) = \mathbf{p}(t) \tag{3.206}$$

with the time t and element contributions from

- element mass matrices $\mathbf{M}_e$ according to Eq. (3.104),
- element nodal displacements $\boldsymbol{v}_e$ according to, e.g., Eq. (3.74) or (3.86),
- element internal nodal forces $\mathbf{f}_e$ according to Eq. (3.102),
- element nodal loads $\mathbf{p}_e = \bar{\mathbf{p}}_e + \bar{\mathbf{t}}_e$ according to Eqs. (3.105, 3.106).

in the case of beams. Nodal loads $\mathbf{p}(t)$ are generally defined as a function of t. Equation (3.206) forms a system of ordinary differential equations of the second order in time t. Thus, initial conditions have to be prescribed for the nodal displacements and velocities at a time $t = 0$. Internal nodal forces are given by

$$\mathbf{f}(t) = \mathbf{K} \cdot \boldsymbol{v}(t) \tag{3.207}$$

in the case of linear material behavior and small displacements with the element contributions to the stiffness matrix $\mathbf{K}_e$ in analogy to Eq. (3.103). This leads to

$$\mathbf{M} \cdot \ddot{\boldsymbol{v}}(t) + \mathbf{K} \cdot \boldsymbol{v}(t) = \mathbf{p}(t) \tag{3.208}$$

instead of Eq. (3.206). Two fundamental solution approaches are given:

- Modal decomposition
- Direct integration in time

Modal decomposition presupposes constant symmetric matrices $\mathbf{M}$, $\mathbf{K}$ and at first neglects loading $\mathbf{p}(t)$. An oscillation may occur with such a system due to initially prescribed displacements or velocities. The system

$$\mathbf{M} \cdot \ddot{\boldsymbol{v}}(t) + \mathbf{K} \cdot \boldsymbol{v}(t) = 0 \tag{3.209}$$

of ordinary differential equations of second order in time t is solved by

$$\boldsymbol{v} = \boldsymbol{\xi} \sin \omega t \tag{3.210}$$

with a constant vector $\boldsymbol{\xi}$ and a constant number ω. They will come out as eigenvector and *circular natural frequency*. Circular natural frequency and *natural period* are related by

$$T = \frac{2\pi}{\omega} \tag{3.211}$$

A generalized matrix eigenvalue problem is derived from Eqs. (3.209, 3.210) with

$$\mathbf{K} \cdot \boldsymbol{\xi} = \omega^2 \mathbf{M} \cdot \boldsymbol{\xi} \tag{3.212}$$

This has n solutions $\boldsymbol{\xi}_i$, ω_i, $i = 1, \ldots, n$ for a system with n nodal degrees of freedom whereby the length of a vector $\boldsymbol{\xi}_i$ remains undetermined. For the solution methods for the generalized matrix eigenvalue problem, see [3, 10., 11.].

The eigenvectors $\boldsymbol{\xi}_i$ constitute a matrix $\boldsymbol{\Xi}$ used for transformations into the modal space. Firstly, the transformation $\tilde{\boldsymbol{v}} = \boldsymbol{\Xi} \cdot \boldsymbol{v}$ is applied. Secondly, the transformations $\tilde{\mathbf{K}} = \boldsymbol{\Xi}^T \cdot \mathbf{K} \cdot \boldsymbol{\Xi}$ and $\tilde{\mathbf{M}} = \boldsymbol{\Xi}^T \cdot \mathbf{M} \cdot \boldsymbol{\Xi}$ each lead to a diagonal matrix. Thirdly, multiplying Eq. (3.208) from left with $\boldsymbol{\Xi}^T$ decouples this set of equations into n single degree of freedom systems of second differential order in time. This decoupling extremely facilitates the solution. This short description outlines *modal analysis*. Only some aspects of modal analysis, which is a powerful tool for all types of structures, can be given within this context. A comprehensive presentation is given by, e.g., [43].

A few basic items of linear structural dynamics remain to be added. The smallest circular natural frequency ω_1 is determined through the *Rayleigh quotient*

$$\omega_1 = \min \left(\sqrt{\frac{\bar{\boldsymbol{v}}^T \cdot \mathbf{K} \cdot \bar{\boldsymbol{v}}}{\bar{\boldsymbol{v}}^T \cdot \mathbf{M} \cdot \bar{\boldsymbol{v}}}} \right) = \frac{2\pi}{T_1} \tag{3.213}$$

with an appropriate displacement vector $\bar{\boldsymbol{v}}$. This also gives the largest natural period T_1 which is relevant for the estimation of dynamic situations. In the case of a single-degree of freedom system – a mass m connected with a base through a spring with stiffness k – this leads to the well-known relation

$$\omega = \sqrt{\frac{k}{m}}, \quad T = 2\pi \sqrt{\frac{m}{k}} \tag{3.214}$$

In the case of multidegree of freedom systems with $n > 1$, as is given within this framework, ω_1 and T_1 may be approximately determined with a $\bar{\boldsymbol{v}}$ resulting from a quasistatic analysis with dead loading.

Finally, the relation for the largest natural period of a simple single span hinged beam shall be derived. The base is given with the homogeneous differential equation of beam bending (Eq. (3.61))

$$m\,\ddot{w} + EJ\,w'''' = 0 \tag{3.215}$$

with a bending stiffness EJ. This is solved by

$$w(x,t) = \sin \frac{\pi\,x}{L}\, \sin \omega t \tag{3.216}$$

with a span L and leads to

$$\ddot{w} = \frac{\partial^2 w}{\partial t^2} = -\omega^2 \sin \frac{\pi\,x}{L}\, \sin \omega t, \quad w'''' = \frac{\partial^4 w}{\partial x^4} = \frac{\pi^4}{L^4} \sin \frac{\pi\,x}{L}\, \sin \omega t \tag{3.217}$$

Thus, boundary conditions $w(0,t) = w(L,t) = 0$ and $EJ\,w''(0,t) = EJ\,w''(L,t) = 0$ are fulfilled. Furthermore, combining Eqs. (3.215, 3.217) yields

$$\omega = \frac{\pi^2}{L^2} \sqrt{\frac{EJ}{m}} \tag{3.218}$$

and with Eq. (3.211) the longest natural period of a single span hinged beam

$$T = \frac{2L^2}{\pi}\sqrt{\frac{m}{EJ}} \tag{3.219}$$

This is a useful relation to derive reference values for the longest natural period of beams. The reciprocal $\nu = 1/T$ gives the largest natural frequency, i.e., the number of cycles of a structure's free oscillations per time unit.

The application of modal analysis is restricted to linear or linearized problems. Such a restriction does not apply if the basic Eq. (3.206) is directly integrated in time. A well-known method for numerical integration in time is given by the Newmark method, see Section 1.6 and Eq. (1.97). This may immediately be applied to Eq. (3.206) and is demonstrated with the following example.

Example 3.9 Beam under impact load
We refer to Example 3.2 with the same geometry and boundary conditions. A sudden concentrated single point load or *impact* is applied in mid span. A linear elastic behavior is assumed in a first approach to demonstrate basic characteristics of dynamic behavior under impact. Following data are chosen:

- Young's modulus is assumed with $E = 33\,000\,\mathrm{MN/m^2}$ and the the specific *weight* with $25\,\mathrm{kN/m^3}$. With an earth acceleration $g \approx 10\,\mathrm{m/s^2}$ this leads to a specific *mass* $\varrho = 0.025/10 = 2.5 \times 10^{-3}\,\mathrm{MNs^2/m^4}$ and with the cross-sectional area $A = 0.2 \cdot 0.4\,\mathrm{m^2}$ to a beam mass per length $m = 0.2 \times 10^{-3}\,\mathrm{MNs^2/m^2}$.

- With the given parameters the longest natural period is determined with $T = \frac{2L^2}{\pi}\sqrt{\frac{m}{EJ}} = 0.038\,\mathrm{s}$ and a frequency $\nu = 26\,\mathrm{Hz}$.

The point load is characterized by an amplitude P_0 and a time variation function

$$P(t) = P_0\, f(t) \tag{3.220}$$

The time function is chosen as a step function with limited duration

$$f(t) = \begin{cases} 1 & \text{for} \quad t \le t_d \\ 0 & \qquad\quad t > t_d \end{cases} \tag{3.221}$$

Thus, loading is characterized by the parameters P_0, t_d. Values $P_0 = -0.07\,\mathrm{MN}$ and $t_d = 0.1\,\mathrm{s}$ are used for the linear elastic reference case.

The spatial discretization is performed with $n_E = 20$ extended two-node Bernoulli beam elements, see Section 3.3.2. The Newmark method, see Section 1.6, is used for time integration with a time step $\Delta t = 0.001\mathrm{s}$. The investigated time span is chosen with $0.06\,\mathrm{s}$ which has to be related to the longest natural period, see above.

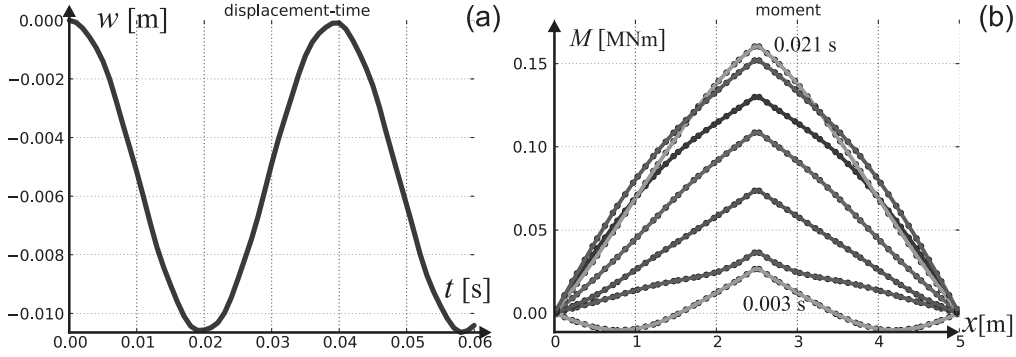

Figure 3.21: Example 3.9 linear elastic (a) Mid-span deflection with time. (b) Moments along beam until the first maximum deflection.

Figure 3.21a shows the computed mid-span deflection during time with the following characteristics:

- A cosine-shaped oscillation occurs.
- The maximum deflection doubles with an absolute value of 0.0106 m compared to the deflection value 0.0053 m caused by a quasistatic loading P_0.

In the same way maximum internal forces are doubled compared to the quasistatic case. Figure 3.21b shows the bending moments along the beam in certain time steps up to the time 0.02 s when the first mid-span maximum is reached. The following points are remarkable:

- Internal forces do not immediately follow the load due to inertial effects.
- There is no longer a triangular course due to a wave propagation effect of moments. In the beginning moments are initiated in the impact point, while the support areas are unaffected. In the following period moment waves travel along the beam and bring the whole beam into action.

Impact loads often have a short duration. Thus, a small parameter study is performed with varying load duration t_d and constant load amplitude $P_0 = -0.07\,\text{MN}$. Figure 3.22a shows the computed maximum mid-span deflections related to the quasistatic deflection depending on t_d related to the longest natural period. If we consider a very short load duration time, e.g., $t_d = 0.001\,\text{s}$, the beam gets only roughly 20% of the quasistatic moment. Or in other words, it may sustain five times the original load to have the same internal forces. This is generalized by the following conclusion:

- Very short loadings are compensated by inertia and only partially result in internal forces.

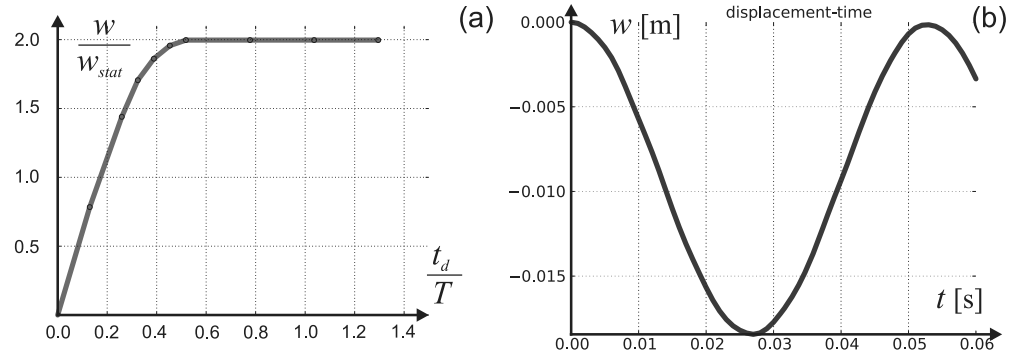

Figure 3.22: Example 3.9 (a) Related maximum deflection depending on related load duration time (b) RC deflection time curve.

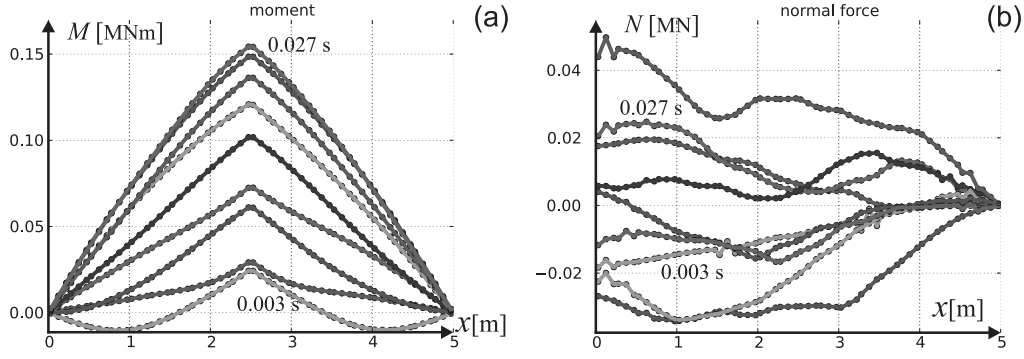

Figure 3.23: Example 3.9 RC (a) Moments along beam until first maximum displacement. (b) Normal forces along beam.

Finally, we consider the original reference case $P_0 = -0.07\,\text{MN}$ and $t_d = 0.1\,\text{s}$ but with a *nonlinear RC section* instead of linear elastic behavior. Material properties and reinforcement are chosen as in Example 3.2 with an additional reinforcement $A_{s2} = 12.57\,\text{cm}^2$, $d_2 = 5\,\text{cm}$ on the upper side. The computation leads to the following results:

- Figure 3.22b shows the mid-span displacement during time. Due to the reduced stiffness the period of the oscillation grows, compare Fig. 3.21a. Maximum mid-span displacement grows to 0.019 m, roughly a doubling occurs compared to the linear elastic case.
- Figure 3.23a shows the bending moments along the beam up to the time 0.027 s when first mid-span maximum is reached. The same moments occur with some time shift compared to the linear elastic case, see Fig. 3.21a.
- In the case of RC some normal forces arise without normal force loading, see Fig. 3.23b. This is caused by the beam's movement in the longitudinal direction due to cracking, which is constrained by the beam's inertia.

– The ultimate limit state is not reached for the given load with maximum absolute values of concrete strain $\epsilon_c \approx -1‰$ and $\epsilon_s \approx 2‰$.

The characteristics of the beam's response are to a large extent determined by the time variation function $f(t)$, see Eq. (3.220). The direct integration in time allows for arbitrary characteristics. A harmonic type would potentially lead to a *resonance* if the excitation frequency is near the natural periods. This effect may occur both for linear and nonlinear behavior.

End Example 3.9

Another aspect of dynamics is *damping*. Damping leads to a *dissipation of energy*. A first model of dissipation has already been given by viscosity, see Fig. 2.8. Dissipation may be treated on the material level and on the system level.

An example of dissipation on the material level has been given by the cyclic behavior of steel, see Fig. 2.10b. This is implicitly covered by the incremental material description (Eq. (1.50)) leading to different tangential stiffness in the case of loading and unloading and thus to energy dissipation within cycles of stress–strain histories.

Dissipation on the system level can be treated in analogy to Eq. (2.21) describing a Kelvin–Voigt element which is extended with a term for mass inertia. This extension is introduced in the generalized form (3.208)

$$\mathbf{M} \cdot \ddot{\boldsymbol{v}}(t) + \mathbf{C} \cdot \dot{\boldsymbol{v}}(t) + \mathbf{K} \cdot \boldsymbol{v}(t) = \mathbf{p}(t) \tag{3.222}$$

with a viscosity matrix $\mathbf{C}$. For aspects determining $\mathbf{C}$ in the case of structural systems and solution methods for Eq. (3.222) see, e.g., [3, 9.3].